Design and Test of a High Speed Actuator for Gas Mixing and Flow Control Applications

Todd D. Batzel
Pennsylvania State University, Altoona College
tdb120@psu.edu

Christopher R. Martin
Pennsylvania State University, Altoona College
crm28@psu.edu

Dimitris W. Kiaoulias
Pennsylvania State University, Altoona College
dwk5403@psu.edu

Matthew J. Cowler
Pennsylvania State University, Altoona College
mjc5921@psu.edu

Abstract

This paper describes the design, prototyping, and testing of an actuator to be used as a high-speed valve for gas mixing. The function of the actuator is to rapidly switch a gas flow on and off using pulse width modulation (PWM). A successful implementation of this actuator will allow regulation of gas flow without the need for sensor feedback.

In the application, the actuator PWM frequency must be sufficiently high so that pressure ripple is minimal downstream of the valve, and the actuator opening and closing times must be fast relative to the PWM period. Furthermore, the actuator must develop sufficient force to overcome high pressures opposing the opening of the valve. These restrictions imply that some combination of a lightweight operator and a high actuator force are requirements of the design. For this reason, a permanent magnet voice coil arrangement is a leading candidate for the actuator topology.

The electromagnetic actuator design is initially performed using magnetic equivalent circuit analysis and then confirmed by more precise finite element analysis (FEA) computations. The design yields actuator parameters such as actuator force per unit current, coil inductance, coil resistance, and magnetic flux densities at various locations in the flux path. These parameters are sufficient to allow an estimation of valve switching characteristics. The prototyping and assembly of the actuator is described. Finally, the gas mixing system's overall performance is tested to validate the effectiveness of the actuator design.

Proceedings of The 2018 IAJC International Conference
ISBN 978-1-60643-379-9

Introduction

This paper presents the design, implementation, and test results of an actuator to be operated in a high-speed digital valve for gas mixing applications. The proposed high-speed actuator is a critical component of a novel digital control system for mixing multiple gases without the need for feedback measurements (Martin & Batzel, 2018). In this application, the actuator must rapidly switch the flow of a pressured gas fully on and off at frequencies of at least 50 Hz to minimize ripple in the downstream gas pressure.

In the study, major design factors such as the physical dimensions and the static and dynamic operating requirements are first analyzed so that an appropriate actuator topology may be selected. With the actuator topology identified and static and dynamic force requirements established, the magnetic circuit components, geometry, and materials are initially analyzed using magnetic equivalent circuits. Airgap, permanent magnet, steel yoke dimensions, and magnetic characteristics are used to compute the airgap magnetic flux density. The computed airgap flux density is then used to determine the number of voice coil turns as well as the conductor size required to match the coil to the desired operating voltage. The developed actuator force is computed as well as the electrical time constant of the voice coil. The actuator design is then verified with a more accurate FEA.

The construction of the actuator prototype and its integration into the valve assembly is then presented. Laboratory tests performed are then used to confirm the force production capability of the actuator. Finally, dynamic testing of the prototype assembly as a digital valve is performed to verify the suitability of the actuator in its intended application.

Actuator Requirements and Constraints

The first step in the actuator design is to identify the requirements, which, coupled with the geometric constraints, will allow selection of the actuator topology. Using this topology, the magnetic and electric loading points can be selected, and electromagnetic computation and analysis can then be performed. This process is iterated as necessary until a satisfactory solution is obtained.

Actuator requirements include both static and dynamic force production capability. The actuator must be able to provide enough static force (F_{stat}) to overcome that of the gas pressure. This static force is the product of the gas pressure P_{gas} and effective cross-sectional area of the valve seat A_o. The nozzle dimensions shown in Figure 1 are used to obtain an effective valve seat area. Using a maximum delivery gas pressure of 125psi yields a required actuator static force (F_{stat}) of 6.8N. During operation, the full 125psi is not typically across the valve so this static force computation represents a worst-case analysis.

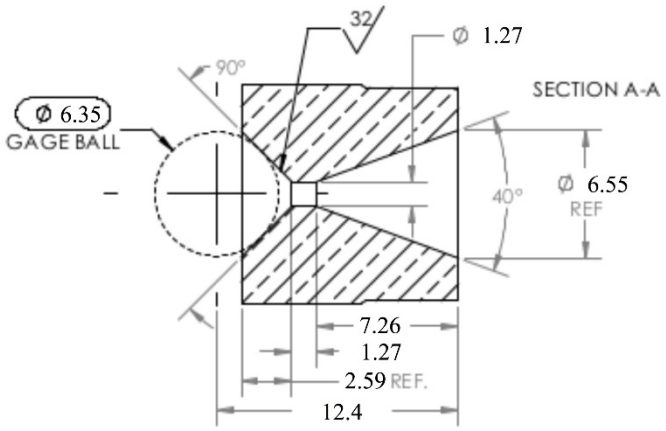

Figure 1: Valve seat (dimensions in mm)

The actuator must also be capable of opening and closing the valve in 2 ms. During valve opening, the actuator must overcome the static force (F_{stat}) as well as provide the required dynamic accelerating force (F_{acc}). The dynamic motion profile for the valve operator is shown in Figure 2. The maximum stroke length is limited by an adjustment screw nominally set to limit motion to .4 mm. The dynamic accelerating force is the product of the operator mass and the required acceleration. Initially assuming a total operator mass of 0.03kg, a dynamic force of 6N is required. In this case, the actuator must provide a maximum force of 12.8N to open the valve, where the operator must initially overcome the static force as well as provide the accelerating force. The static force, however, vanishes as the valve opens, so that closing the valve, only requires the accelerating force. Clearly, keeping the mass of the operator low is critical in keeping the dynamic forces to an achievable level. This constraint has led to the selection of a voice coil type actuator topology.

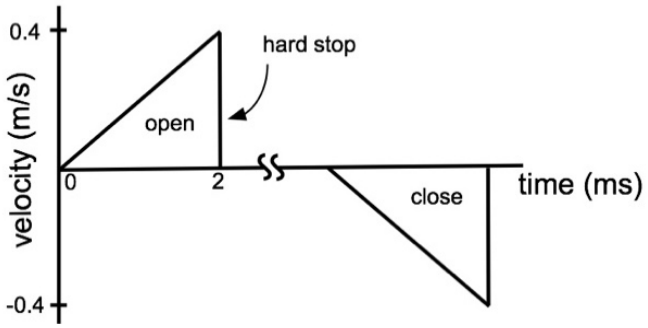

Figure 2: Motion profile of the operator

Voice Coil Actuator

The voice coil topology is ideal in applications that require high frequency operation or fast acceleration because of its fast electrical and mechanical time constants (Sung & Kim, 2018; Roemer, Bech, Johansen, & Pedersen, 2015). A voice coil type actuator (VCA), as shown in Figure 4, uses a permanent magnet, whose field interacts with a coil winding current to produce a force that is proportional to the applied coil current, and generally yields a linear force per unit current characteristic. The direction of the force can be reversed in a voice coil by reversing the direction of the coil current. The developed actuator force can be estimated by using

$$F_{act} = Bli \tag{1}$$

Where F_{act} is the force in Newtons, *B* is the magnetic flux density perpendicular to the current, *l* is the total length of the wire (the product of the number of turns, *N*, and the circumference of the coil), and *i* is the current in the coil. A voltage *e* is also induced in the coil when it is in motion:

$$e = Blu \tag{2}$$

Here *u* is the velocity of the coil relative to the magnetic field.

Design of Voice Coil Actuator

A good starting point in sizing a voice coil actuator is to select an appropriate shear stress target. Air gap shear stress (τ) is often used in electric machine design as a sizing metric since it is generally similar even for different sizes of machines of the same topology (Beaty & Kirtley, 1998; Batzel, Skraba & Massi, 2014). For the voice coil actuator, the shear stress is a measure of the actuator force per unit surface area of the airgap. As a point of reference, common permanent magnet motor designs without special provisions for forced cooling have an airgap shear stress in the range from 3.5 to 14 kPa (Hanselman, 2006). For the permanent magnet actuator design, an airgap shear stress in that same range is selected - 10kPa. The airgap shear stress is represented by

$$\tau = \frac{F_{act}}{A_g} \tag{3}$$

Where A_g is the airgap surface area where the coil current is interacting with the permanent magnet field. Using Equation 1 and assuming that the airgap is cylindrical with a radius *r* and a height *h*, the airgap shear stress can be written as

$$\tau = \frac{Bli}{2\pi rh} = \frac{B(2\pi r)i}{2\pi rh} = BZ \tag{4}$$

Where the linear current density *Z* (A/m) is representative of the electrical loading, and the flux density *B* is the magnetic loading of the actuator.

To achieve the target airgap shear stress of 10 kPa, a magnetic loading *B* of .4 Tesla is selected. This is a reasonable magnetic loading that is achievable for neodymium type

(NdFeB) permanent magnets operating near its point of maximum energy product. To get maximum flux density per unit volume of permanent magnet material, the permanent magnet should be operated near this point of maximum energy product (Boldea & Nasar, 2005). Also, from Equation 4, the target shear stress and magnetic loading parameters will require an electrical loading of 25,000 A/m.

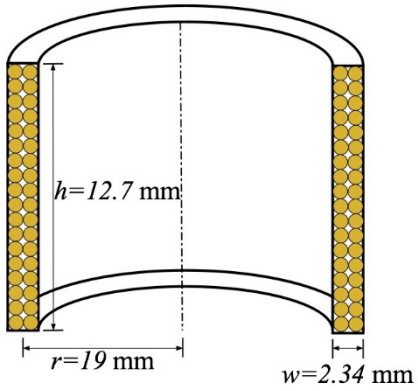

Figure 3: Actuator coil dimensions

The coil dimensions and airgap length are now computed using the active airgap area A_g, the linear current sheet density *Z*, and a conductor current density *J*. Using Equation 3 and an actuator force F_{act}=15 N to provide headroom beyond the required maximum torque of 12.8 N, the required active airgap area to achieve the targeted airgap shear stress is 1.5×10^{-3} m^2. As shown in Figure 3, the active airgap area is

$$A_g = 2\pi rh \tag{5}$$

To achieve the required airgap area A_g, the coil radius *r* is selected to be .019m (¾ in), and the coil height *h* is .0127m (½ in). This choice of dimensions was made in part to keep the overall actuator profile comparable with that of typical gas metering valves.

To estimate the coil width *w*, shown in Figure 3, a conductor current density *J* of 15 A/mm^2 is selected. This current density is similar to that commonly used in actuators (Yatchev, Hinov, Balabozov, & Krasteva, 2011) and should not result in excessive temperature rise (Soong, 2016) in this application. Considering the copper fill factor σ of the coil, which is estimated to be 0.71 for a multi-layer packed coil where the insulation adds an extra 10% diameter to the conductor (MS Wire, 2014), the width of the coil is

$$w = {}^{Z}/_{J\sigma} \tag{6}$$

This results in a required coil width of 2.34 mm. A clearance of .42mm on each side of the coil gives a total airgap length of 3.18 mm (1/8 in). Using the current density of 15 A/mm^2, a 24 gauge wire (diam .51mm), for example, can carry 3.1 A rms of current.

Magnetic Equivalent Circuit Analysis of VCA

Given the computed airgap and coil dimensions from the previous section, a magnetic equivalent circuit (MEC) analysis is now performed to identify dimensions for the permanent magnet and iron yoke. Magnetic equivalent circuit analysis allows for rapid computation of the actuator operational parameters so that the design can be quickly iterated as necessary until satisfactory characteristics are achieved.

There are many options for the selection and placement of the VCA permanent magnet. Although an axially magnetized cylindrical permanent magnet in the inner yoke, and an radially magnetized ring magnet located at the airgap were considered, the axially magnetized ring magnet type, as shown in Figure 4, was ultimately selected. This choice was made because it simplifies assembly and is available off-the-shelf in a variety of dimensions. Figure 4 illustrates the selected voice coil actuator topology, where the airgap and coil dimensions were determined in the previous section, and the magnet dimensions shown were obtained after many iterations of magnetic equivalent circuit analysis, which is now described.

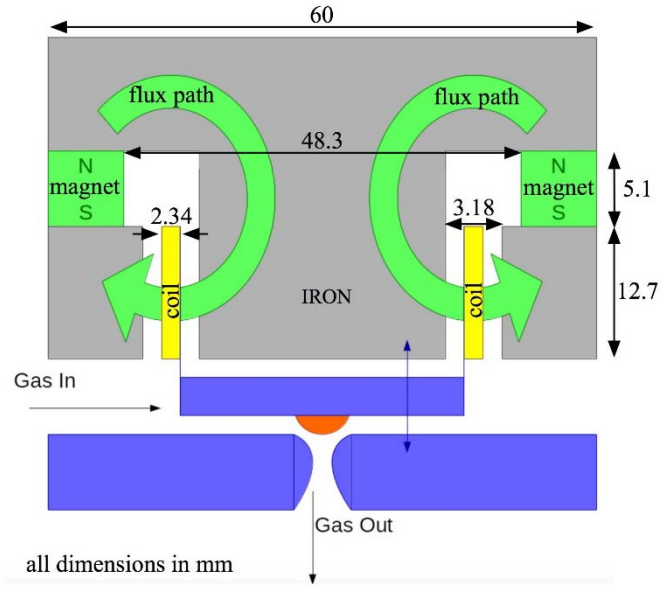

Figure 4: Voice Coil Actuator Sketch

Using the simplifying assumption that the iron yoke permeability is infinite, the sum of magneto-motive force around any of the flux paths shown in Figure 4 yields

$$H_g = -\frac{l_m}{l_g} H_m \tag{7}$$

Where l_m and l_g are the lengths of magnetic flux path in the magnet and airgap, respectively. The field intensity in the magnet and airgap are represented by H_m and H_g, respectively. The flux density *B* in the airgap is $B_g = \mu_0 H_g$, where μ_0 is the magnetic permeability of free space. Since the magnetic flux ϕ is continuous in the paths shown in the figure,

$$\phi = A_m B_m = A_g B_g \tag{8}$$

Where *A* is the cross-sectional area in which magnetic flux flows in the magnet and airgap, and B_m is the flux density in the permanent magnet. From Equation 8,

$$B_g = \frac{A_m}{A_g} B_m \tag{9}$$

From Equations 7 and 9,

$$B_m = -\mu_0 \left(\frac{A_g}{A_m}\right)\left(\frac{l_m}{l_g}\right) H_m \tag{10}$$

The intersection of Equation 10 and the load line of the magnet B-H characteristic curve defines the operating point of the permanent magnet. In the case of NdFeB (grade 40) magnets, which are linear in the 2nd quadrant of the B-H curve, the B-H normal curve at 60 degrees C is represented by

$$B_m = 1.09\mu_0 H_m + 1.2 \tag{11}$$

The solution of Equations 10 and 11, using the gap dimensions previously computed ($A_g = 1.5 \times 10^{-3}\text{m}^2$ and $l_g =$ .00318 m.), can be used to determine suitable magnet dimensions. After several iterations, the magnet dimensions given in Table 1 were selected.

Using the airgap dimensions determined previously ($A_g = 1.5 \times 10^{-3}\text{m}^2$ and $l_g =$ .00318 m), Equations 10 and 11 can be solved to obtain practicable magnet dimensions. After multiple iterations of this magnetic analysis, a magnet of dimensions given in Table 1 was selected. The dimensions were selected in part based on off-the-shelf availability of the magnet.

For the selected magnet, Equations 10 and 11 yield an operating point of $B_m = .82\ T$ and an airgap magnetic flux density $B_g = .54\ T$. This resulting airgap flux density is well above the target magnetic loading of .4 T. It should also be noted that the MEC analysis, though it provides a very quick iterative solution for the magnetic circuit dimensions, ignores flux

Table 1. Ring magnet dimensions.

Parameter	Value
Outer Radius	29.97 mm
Inner Radius	24.13 mm
Thickness	5.1 mm
Material	NdFeB Grade 40
A_m	$9.926 \times 10^{-4}\text{m}^2$
l_m	.00508 mm

leakage paths and the iron's finite permeability. Despite the known limitations of MEC, it serves as a starting point for an FEA solution that will yield more accurate results.

Coil Design and Parameters

The target electrical loading of *Z*=25,000 A/m and the coil dimensions shown in Figure 3 are now used to specify the coil construction and compute its electrical characteristics. The number of Ampere-Turns ($\mathcal{F}$) required of the coil is

$$\mathcal{F} = Zh = 317.5\ A - T \tag{12}$$

This result suggests that the coil could be constructed with *N* turns of conductor designed to carry 317.5/*N* Amperes of current. The trade-off is clearly that of coil current and induced voltage in the coil. Since it is standard for gas metering valves, 24 V DC is selected as the supply voltage for this application. The voltage induced in the moving voice coil, therefore should be below the supply voltage of 24V by enough margin so that the current control can rapidly reverse or change the actuator coil current. The voltage induced in the moving voice coil is computed using

$$e_{coil} = \frac{d\lambda_{coil}}{dt} \tag{13}$$

Where λ_{coil} is the magnetic flux linking the coil. The maximum flux linking the coil in the neutral position as shown in Figure 4 will be $0.5NB_gA_g = N\ (4.1 \times 10^{-4})$ Webers. Using a slightly overstated stroke length of 1 mm, an overall coil height of 12.7mm, and neglecting flux fringing as an approximation, the flux linkage is reduced to approximately $N(3.47 \times 10^{-4})$ Webers as coil turns move outside of the airgap (at bottom of Figure 4) and flux flowing near the top of the gap no longer link any turns. If the stroke occurs in 2ms, the approximate induced coil voltage during the motion will be

$$e_{coil} = \frac{.N(.63\times10^{-4}\ W)}{.002\ s} = .032N\ \text{V} \tag{14}$$

Using Equation 14, a coil with *N*=100 turns is selected for the design. With 100 turns, the induced coil voltage during voice coil motion will be a peak value of 3.2V, which provides ample voltage headroom for a current controller operating with a 24V dc supply.

To fit 100 conductor turns into the coil dimensions shown in Figure 3, a 24-gauge magnet wire, with a conductor area of $A_{wire} = .205\ \text{mm}^2$ is selected. For the estimated copper fill factor of 71% and the available cross-sectional area for the conductors of 29.7 mm^2, 100 24-gauge conductors will fit into the designated coil cross-section.

The resistance of the coil is computed from

$$R_{coil} = \frac{\rho l_{coil}}{A_{wire}} = \frac{(1.68\times10^{-8}\Omega-\text{m})(2\pi)(.019\text{m})(100)}{.205\times10^{-6}\ \text{m}^2} = 1\ \Omega \tag{15}$$

Where ρ is the conductivity of copper, and l_{coil} is the total length of wire in the coil. Similarly, the coil inductance is computed from

$$L_{coil} = \frac{N^2}{(\mathcal{R}_g + \mathcal{R}_m)} \tag{16}$$

Where $\mathcal{R}_g$ and $\mathcal{R}_m$ represent the magnetic reluctance of the airgap and magnet. The reluctances are

$$\mathcal{R}_g = \frac{l_g}{\mu_0 A_g} = 1.69 \times 10^6\, H^{-1} \quad ; \quad \mathcal{R}_m = \frac{l_m}{1.09\mu_0 A_m} = 3.74 \times 10^6\, H^{-1} \tag{17}$$

giving a coil inductance $L_{coil} = 1.84\ mH$. Finally, the electrical time constant of the coil

$$\tau = \frac{L_{coil}}{R_{coil}} \tag{18}$$

is found to be 1.84 ms. Given the considerable voltage headroom, the 24V DC supply can drive the coil current to rated values in fraction of the electrical time constant. Therefore, the electrical time constant is not expected to limit the dynamic performance requirements of the actuator.

Finite Element Analysis of Voice Coil Actuator

The analytical MEC method used for initial characterization of the actuator is based on several simplifying assumptions. FEA, though much more time and computationally intensive, provides very accurate results and therefore can be used to confirm or modify the initial MEC solution as needed. In this section, FEA tools are used to evaluate and confirm the proposed actuator design.

The axisymmetric property of the actuator design is exploited so that a 2D FEA model can be used in the analysis. Figure 5 shows the actuator model, as well as the FEA solution for the magnetic flux lines and the magnetic flux density, where low carbon AISI 1018 steel is used for the yoke. From the previous section, the MEC analysis predicted a flux density B_m in the permanent magnet of .82 T. This compares rather well with the FEA solution that predicts a permanent magnet operating point B_m of .9 T. However, the MEC predicts of an airgap flux density B_g of .54 T, which is significantly higher than the FEA computed airgap flux density of .3 T. The difference in predicted airgap flux densities can be explained by the magnetic flux lines shown in Figure 5 that do not take their intended path through the airgap. This so-called flux leakage is not considered by MEC analysis, resulting in a higher the airgap flux density prediction. A gauss probe inserted in the airgap of the prototype actuator was later used to confirm that the actual airgap flux is in very close agreement with the FEA result of .3 T. Figure 5 also demonstrates that the flux density in the steel yoke does not exceed 1 T at any location, which is well below its saturation point of about 1.5 T.

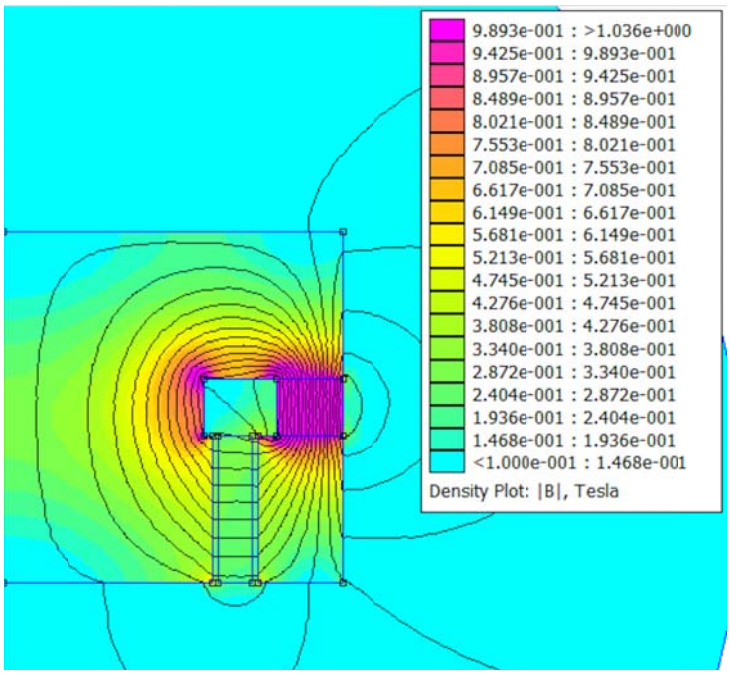

Figure 5. FEA Model and Magnetic Characteristics Solution (Zero Current)

In Figure 6, the airgap flux density is shown along the length of the airgap for various coil currents. When the coil is not energized, the permanent magnet provides a rather uniform magnetic flux density along the length of the gap with the expected reduction near the edges. As seen in the figure, current in the coil produces an armature reaction field that slightly alters the airgap flux density. Positive coil current produces an armature field in the same direction as the permanent magnet, while negative coil current has the opposite effect. This armature reaction effect (Jang & Jeong, 2001) yields a slightly unbalanced force versus current characteristic as illustrated in Figure 7, which shows that positive current produces a slightly higher force magnitude. Despite the armature reaction effect, the force per current is nearly linear, with a force sensitivity of 3.92 N/A for positive coil current.

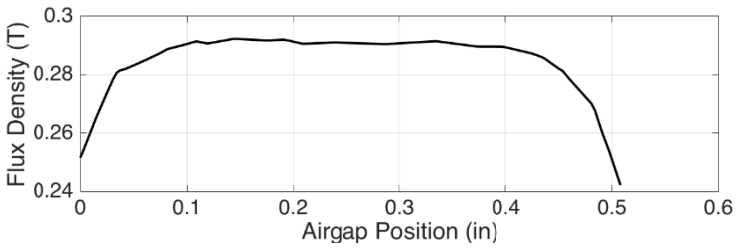

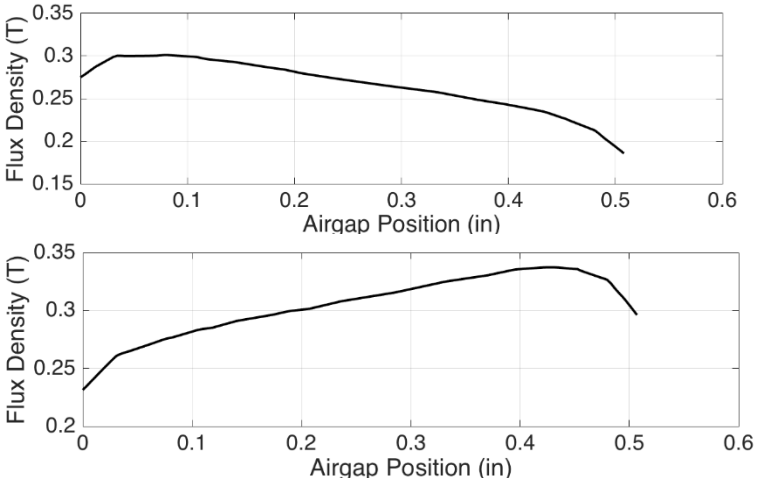

Figure 6. Airgap Flux Density for Coil Current of 0A (top), -3A (mid.), and +3A (bot.)

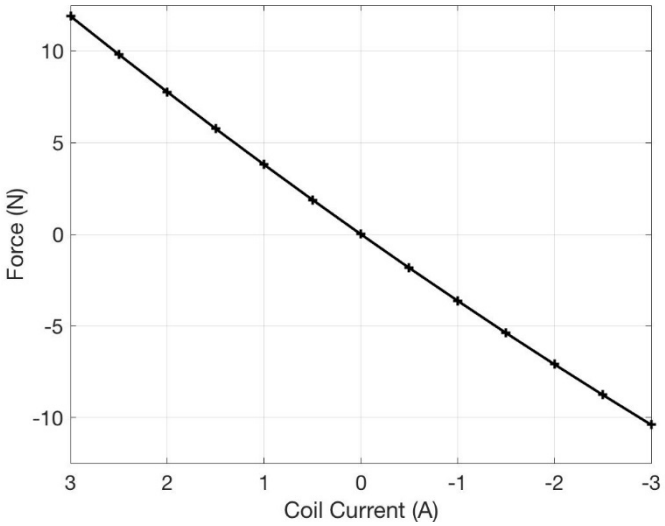

Figure 7. FEA Predicted Force versus Coil Current

The voice coil electrical parameters are also computed using the FEA, and the results are presented in Table 2. Note that the FEA computed parameters are in very close agreement with those obtained with the MEC method.

Table 2. FEA Computed Electrical Parameters

Property	**Value**
Coil Inductance	2.2 mH
Coil Resistance	1.09 ohms
Coil Power Dissipation	9.81 W (at 3 Amps)

Coil Time Constant	2 ms

Fabrication of Actuator Prototype

The coils were wound using AWG 24 magnet wire, wound on top of a Nomex paper layer on the inner diameter to improve strength. The coil design calls for 100 turns, which was implemented by four layers of packed wire with 25 turns per layer. This coil arrangement was selected to fit into the allotted coil space as indicated in Figure 3. The valve operator was then attached to the inner diameter of the Nomex using an epoxy adhesive. The constructed voice coil and valve operator is shown in Figure 8.

Figure 8. Voice Coil and Operator (left) Inserted into Outer Shell Assembly (right)

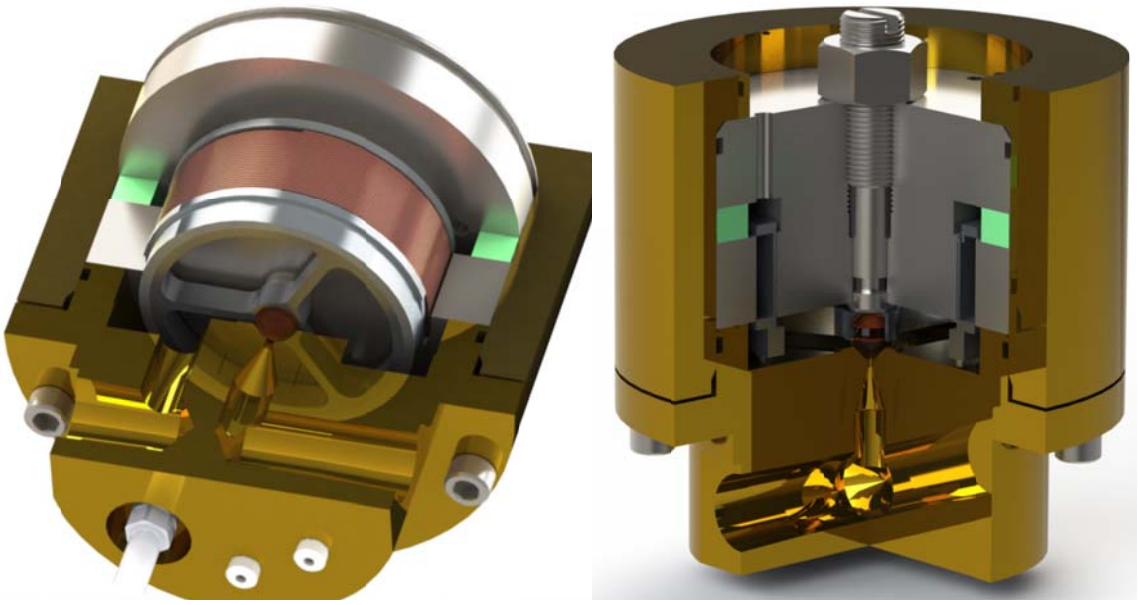

Figure 9. Sectioned Renderings of the Prototype Actuator

The yoke of the prototype actuator was constructed with a machined block of AISI 1018 Steel that was annealed after machining. Figure 9 shows a sectioned rendering of the prototype actuator. A NdFeB grade 40 ring magnet (rendered in green) magnetized in the axial direction is placed between a T-shaped steel yoke and a steel ring (steel rendered in white//gray), forming an annulus with a radial magnetic field in the airgap. The sapphire ball (red) is pressed into an aluminum yoke (silver), and a coil of 100 turns of AWG 24 magnet wire forms a coil approximately 0.5 inches long. The valve body is machined from three-inch diameter brass (rendered in bronze). The conical valve seat is machined as a separate part and pressed into the valve body as shown. The total mass of the operator (sapphire ball, aluminum yoke, and copper coil) is .03kg, which is the value used in computing the dynamic force requirements in an earlier section of this paper.

Actuator and Valve Testing

To confirm the magnetic loading of the prototype actuator, the voice coil was temporarily removed from the yoke so that a gauss probe could be inserted into the airgap. The flux density around the gap was evaluated at the midpoint of the gap length, and along the height of the airgap. Except for near the boundaries of the gap height, the flux density was found to be uniform at a level of approximately .3T, which is in good agreement with the FEA prediction shown in Figure 6 (top).

To measure the force produced by the prototype actuator, the voice coil was supplied with a constant current while a mass attached to the operator was adjusted until the actuator force balanced the gravitational force acting on the mass. The results of this test are shown in Figure 10, which includes a linear fit extended to higher A-T than used experimentally. The linear fit indicates that 11.25N force will be produced for a coil current of 3A in a 100-turn coil. This is in close agreement with the FEA prediction of 11.77N (for +3 Amps). The

scatter of the data points in Figure 10 is attributed to inaccuracies associated with the simple test setup – mainly the inconsistent voice coil positioning within the airgap during the tests. Since the voice coil used in this force test did not have the full 100 turns called for in the design, the unit A-T is used so that results are easily extended to a 100-turn voice coil.

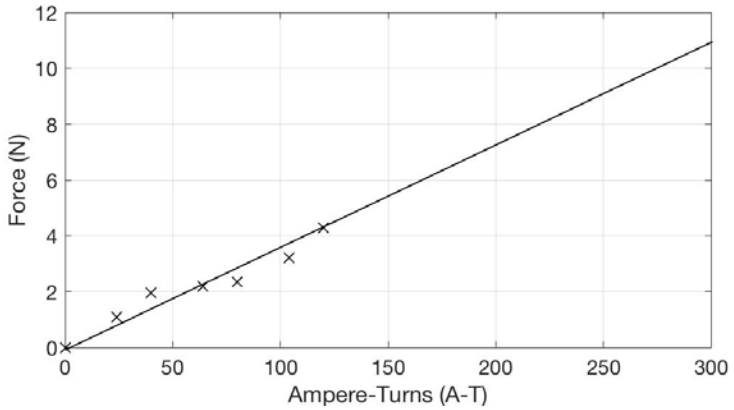

Figure 10. Experimentally Determined Force versus A-T Extrapolated to 300 A-T

Based on the FEA and test results, the goal of producing a peak actuator forces of 12.8N, will require peak coil currents of 3.3 A (assuming the FEA-computed actuator sensitivity of 3.92 N/A). Although this peak current in the selected magnet wire will slightly exceed the conductor current density of 15 A/mm^2, the rms conductor current can kept much lower considering that the peak current is only required briefly when opening the valve.

Finally, the actuator was tested for functionality as a flow valve. For this test, the prototype valve was supplied with 50psig shop air and used to fill a 5 USGal pneumatic reservoir. The voice coil of the actuator was driven with a ±2A square wave with duty cycles between 20% and 80% at 100Hz and below. Flow rate was determined by monitoring the reservoir pressure and temperature over the duration of the test. Figure 11 shows the measured flow rate for various duty cycles applied to the voice coil at a switching frequency of 50 Hz. These tests demonstrate linearity with respect to duty cycle, with an frequency dependent offset due to flow transience (Martin & Batzel, 2018).

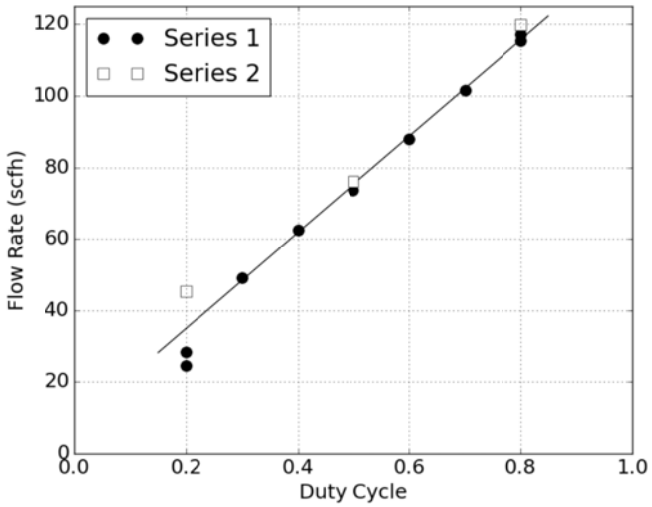

Figure 11. Flow Rate versus Duty Cycle for 50 Hz Valve Switching

Conclusions and Future Work

This paper describes the design methodology, construction, and testing of a high-speed actuator to be used in a novel gas mixing application. The gas mixing application requirements are used to identify actuator design, and the electromagnetic components of the actuator were analytically selected to meet these goals. The initial design was carried out using an iterative magnetic circuit analysis. This was followed up with a confirmation and fine-tuning using magnetic finite element analysis methods. The analysis shows that the proposed actuator design can meet all of the design goals including force, and dynamic switching. Finally, a prototype actuator was constructed, and a successful demonstration of the switched nozzle approach to flow control was performed. Flow data demonstrated linear behavior with respect to the voice coil duty cycle at switching frequencies up to 100 Hz.

In the future, the actuator performance could be further improved by taking steps to reduce the magnetic flux leakage. This could be accomplished in part by increasing the ratio of the permanent magnet thickness relative to the airgap length.

References

Batzel, T. D., Skraba, A., & Massi, R. (2014). Design and test of an ironless axial flux permanent magnet machine using Halbach array. *International Journal of Modern Engineering, 15*(1), 52-60.

Beaty, H. W., & Kirtley, J. L. (1998). *Electric motor handbook*. New York: McGraw-Hill.

Boldea, I. & Nasar, S. A. (2005). *Linear electric actuators and generators*. Cambridge, UK: Cambridge University Press.

Hanselman, D. (2006). *Brushless permanent magnet motor design*. Lebanon, OH: Magna Physics Publishing.

Jang, S. M., & Jeong, S. S. (2001). Armature reaction effect and inductance of moving coil linear oscillatory actuator with unbalanced magnetic circuit. *IEEE Transactions on Magnetics*, *37*(4), 2847-2850.

Martin, C. R., & Batzel, T. D. (2018). Digital feed-forward control of gas mixture with high-speed valve switching. *Proceedings of Manufacturing Science and Engineering Conference 2018*. Paris: Atlantis Press.

MS Wire Industries. (2014). *Bondable magnet wire*. Retrieved from http://www.mwswire.com/pdf_files/mws_tech_book/page8_9_35.pdf

Roemer, D. B., Bech, M. M., Johansen, P., & Pedersen, H. C. (2015). Optimum design of a moving coil actuator for fast-switching valves in digital hydraulic pumps and motors. *IEEE/ASME Transactions of Mechatronics, 20*(6), 2761-2770.

Soong, W. L. (2016). *The art of electric machine research, ch. 2 – Electrical conductors*. Retrieved from http://www.eleceng.adelaide.edu.au/research/power/pebn/art%20of%20emr%20-%20ch2%20conductors%20sep16.pdf

Sung, B. J., & Kim, D. S. (2018). A design method of voice coil type high speed actuator for valve operation. *Proceedings of the 15th International Conference on Electrical Machines and Systems*. Piscatawny, NJ: IEEE.

Yatchev, I., Hinov, K., Balabozov, I., & Krasteva, K. (2011). Static force characteristics of electromagnetic actuators for braille screen. *Facta Univ - Electronics and Energetics*, *24*(2), 157-167.

Biographies

TODD BATZEL received the BS and PhD degrees in Electrical Engineering from the Pennsylvania State University, University Park, in 1984 and 2000, respectively, and the MS degree in Electrical Engineering from the University of Pittsburgh, Pittsburgh, PA, in 1989. Currently, he is a professor of Electrical Engineering at Penn State University, Altoona College. Dr. Batzel may be reached at tdb120@psu.edu.

CHRISTOPHER MARTIN is currently an assistant professor of Mechanical Engineering at Penn State University's Altoona College. Dr. Martin received a BS, MS, and PhD in Mechanical Engineering from Virginia Tech in 2004, 2006, and 2009, respectively. He also holds a certificate in Engineering Education from Virginia Tech. Dr. Martin may be reached at crm28@psu.edu.

DIMITRIS KIAOULIAS is presently an undergraduate student in the BS in electro-mechanical engineering technology (BSEMET) program at Penn State Altoona, Altoona, PA. He may be reached at dwk5403@psu.edu.

MATTHEW COWLER is presently an undergraduate student in the BS in electro-mechanical engineering technology (BSEMET) program at Penn State Altoona, Altoona, PA. He may be reached at mjc5921@psu.edu.